

***In situ* valence modification of Pd/NiO nano-catalysts in supercritical water towards toluene oxidation**

Qingjie Meng^a, Jiajia Liu^a, Xiaole Weng^{*a,b}, Pengfei Sun^a, Jawwad. A. Darr^c and Zhongbiao Wu^{a,b}

^a Key Laboratory of Environment Remediation and Ecological Health, Ministry of Education, College of Environmental and Resource Sciences, Zhejiang University, 310058 Hangzhou, P. R. China.

^b Zhejiang Provincial Engineering Research Centre of Industrial Boiler & Furnace Flue Gas Pollution Control, 388 Yuhangtang Road, 310058 Hangzhou, P. R. China.

^c Department of Chemistry, University College London, Christopher Ingold Laboratories, 20 Gordon Street, London, WC1H 0AJ, UK.

Corresponding author: Tel.: +86 571 88982034; Fax: +86 571 88982034; E-mail: xlweng@zju.edu.cn.

Abstract

Noble metals, e.g. Pd, are often made into hybrid or composite catalysts (with less expensive materials) to oxidize industry-source emitted volatile organic compounds (VOCs) at low temperatures. In general, the loadings of these metals should be optimized to reduce costs, whilst maintaining activity. There exists the possibility to obtain highly active catalysts with low loadings of noble metals by properly tuning the valence state of the metal(s). However, the relationship between the valence state and its effect on catalyst performance is still a matter of debate. In this article, we used

supercritical water (sc-H₂O) in the presence of oxidizing or reducing gases, as a feasible reaction medium to synthesize Pd/NiO hybrid nano-catalysts and *in situ* modify the valence state of Pd. After subjected to a range of analytical techniques, including XRD, H₂-TPR, DRIFT, TPSR, etc., we unveil that the Pd⁰ is more active than PdO_x and metal oxides in the catalytic oxidation of toluene. This is mainly because the stabilized Pd⁰ is capable of dissociating gaseous oxygen (and activating the toluene) at low temperatures and restoring to original state by toluene even with excessive oxygen. The PdO_x, although could desorb active oxygen under a reducing atmosphere and might assist the oxygen spillover from NiO, is difficult to convert into Pd⁰ in an oxygen-rich environment. The developed Pd⁰ dominated catalyst was found to be robust and highly active after ageing test with and without water vapour.

Keywords: *Toluene; Catalytic oxidation; Pd; Supercritical water; Hybrid catalyst.*

1. Introduction

The increasingly stringent legislation on emission standards for volatile organic compounds (VOCs) from polluting factories have led to increased demands in developing reliable and economical technologies for VOC abatement.¹⁻³ Catalytic combustion technology using heterogeneous catalysts to convert VOCs into relatively harmless products (CO₂ and H₂O) has been considered a promising approach to reduce the VOCs emission.⁴⁻⁷ This technique has high demands on catalytic materials, as they need to be cost-effective, durable and active at low temperatures.

Industrial catalysts towards VOCs oxidation generally involve trace amount of noble metal loadings, which are often made into hybrid catalysts (with less expensive

support) in which a synergistic relationship could occur between the two materials. In general, the loading of noble metals should be optimized to reduce the cost, whilst maintaining activity. This involves the proper selection (e.g. Pd is more favourable due to its less expensive than Pt) and the wise modification of the chemical valence of the noble metals. It is well-known that the valence state of noble metals can profoundly affect their VOCs oxidation efficiencies. However, the relationship between the valence state and its effect on catalyst performance is still a matter of debate. Taking Pd for example, some reports^{8,9} assigned the improved activity to the presence of metallic Pd⁰, which can activate gaseous oxygen and thus accelerate the catalytic reaction. However, in other reports¹⁰, the Pd²⁺ (usually as PdO) was considered to be more active than the Pd⁰, whilst others also suggested that a mixture of Pd⁰/PdO was the most active¹¹. Therefore, studies into the mechanistic function of noble metal valence in VOCs oxidation are still demanded. This can assist the proper modification of the noble metal valence to obtain highly active catalysts with low loadings of noble metals.

In the laboratory, the adjustment of noble metal valence is usually achieved through post-synthesis heat-treatments of particles under reducing/oxidizing atmospheres (e.g. H₂, CO or O₂). Such a process, however, can lead to the sintering of surface active particles and/or the encapsulation of them by the support. Under a hydrothermal synthetic condition, the valence adjustment is also not so viable because the insolubility of reducing/oxidizing gases (e.g. H₂, O₂) in ambient H₂O would result in a slow or incomplete reaction between the gases and noble metals (due to the gas-solid-liquid reaction). In this article, we used a flow of supercritical water (sc-H₂O) as a reaction

medium to modify the Pd valence state in a series of Pd/NiO based hybrid nanocatalysts for the catalytic oxidation of toluene. Unlike the ambient H₂O that is a polar solvent, the sc-H₂O is a non-polar solvent, in which the partial breakdown of hydrogen bonds makes it capable of dissolving O₂, H₂, etc ¹². As such, the three-phase reaction between the Pd, H₂O and gas could be effectively reduced into two-phase, which thus accelerates their reaction and makes the *in situ* modification of Pd valence under the hydrothermal condition become feasible. A range of analytical techniques, including XRD, H₂-TPR, DRIFT, TPSR, etc. was applied to explore the mechanistic functions of Pd valences in toluene oxidation. Our goal in this work is to get a better understanding of the Pd valences on the ability of the catalyst towards VOCs oxidation and to provide the guidelines for practically optimizing the noble metals either in loading or in valence for industrial catalysts towards low temperature and durable VOCs oxidation.

2. Experimental

2.1 Materials and Methods

Materials: All chemicals were supplied by Shanghai Aladdin Biochem Technology Co., Ltd (Shanghai, China) and used as obtained. Deionized water was used in all experiments.

Methods: The Pd/NiO hybrid nanocatalysts were manufactured using a three pump hydrothermal flow system (CHFS) ¹³. The reactor, tubing, and components were all made of 316 stainless steel (SwagelokTM). The flow apparatus (see supplementary **Fig. S1**) consists of a metal salt(s) solution HPLC pump (P2), a base solution HPLC pump (P3) and a water HPLC pump (P1). Deionized water was pumped through an

electrical preheating coil (2.5 kW) and heated to an appropriate temperature (450 °C). Separately, two ambient temperature feeds of aqueous metal salt solution [containing the appropriate amounts of Ni(NO₃)₂·6H₂O (0.05 M) and NaOH solution (2 M, in some case with Pd(NH₃)₄Cl₂·H₂O for the syntheses of Pd/NiO hybrid materials) were brought into contact with the sc-H₂O feed in a 3/8" counter-current mixer¹⁴. The mixer was also heated externally via a band heater set at 450 °C. In the mixer, rapid nucleation and crystallization of the reagents occurred. The aqueous suspension of newly formed nanoparticles was then cooled via a water jacket cooler, passed through a 7 μm in-line filter and was collected from the exit of a back-pressure regulator (BPR) valve that was used to maintain the pressure of approximately 23.0 MPa in the system. Flow rates of 10, 10 and 25 mL min⁻¹ were used for the metal salt solution, base solution, and water stream, respectively. Solids were recovered by centrifuging the suspension at 6000 rpm and were then freeze-dried. Since sc-H₂O has a high solubility of O₂¹², this would make the product containing the majority of oxidized Pd species (hereafter denoted as sc-Pd/NiO). As such, to reduce the Pd valence, a reducing agent of formic acid was introduced (as it can be decomposed into H₂, CO₂ and CO in the sc-H₂O)^{15, 16}. The formic acid was added to the aqueous metal salt solution, following a similar procedure to the sc-Pd/NiO. The reduced catalyst was hereafter denoted as sc-Pd/NiO-R. For comparison, a reduced catalyst via post-treatment was synthesized by treating sc-Pd/NiO in H₂, denoted as sc-Pd/NiO-H₂.

2.2 Characterization

X-ray powder diffraction (XRD) was conducted by using a Rigaku D/Max RA diffractometer with the Cu-K α radiation ($\lambda = 0.15418$ nm) at 40 kV and 150 mA. The presence and dispersion of Pd were evaluated by using a model Tecnai G2 F20 S-TWIN (FEI Company, USA) high-resolution transmission electron microscope (HR-TEM, 400 kV accelerating voltage) instrument equipped with a STEM and HAADF. The content of Pd was measured by using an inductively coupled plasma atomic emission spectrometry (ICP-AES, Optima 7300 DV (Perkin Elmer Corporation, USA)). The surface elemental analysis was conducted by using a Thermo ESCALAB 250 XPS instrument with Al-K α radiation (photon energy 1486.6 eV) at 150 W. The signal of adventitious carbon (the binding energy of 284.8 eV) was used to calibrate the binding energy scale. Curve fits were performed using a Shirley background and a Gaussian peak shape with 20 % Lorentzian character. N₂ physisorption at the liquid nitrogen temperature (-195 °C) was conducted via a static volumetric adsorption analyzer JW-BK132F (Beijing Jingweigaobo Technology. Co. Ltd, China). The data were analyzed based on the Brunauer-Emmett-Teller (BET) model. Prior to measurements, all catalysts were degassed at 150 °C for 2 h in vacuum.

Temperature-programmed reduction (TPR) was conducted by using an automatic multi-purpose adsorption instrument TP-5079 (Tianjin Xianquan, China) equipped with a Thermal Conductivity Detector (TCD) and HIDEN QGA portable mass spectrometer (MS). The catalyst (at 0.05 g) was first heated to 200 °C in a flow of 5 vol% O₂/He (at 50 mL min⁻¹) in a tube furnace (Tianjin Xianquan, China) with a dwell time of 1 h and

then allowed to naturally cool to room temperature. Thereafter, the reducing gas (6 vol% H₂/N₂, flow rate 35 mL min⁻¹) was purged in for 30 min and the catalyst was then heated up to 900 °C at a rate of 5 °C min⁻¹. The H₂ consumption was recorded by using the TCD.

The concentration of chemisorbed oxygen species at the surface was determined by Hydro-Oxygen Titration (HOT) method using a TP-5079 instrument. The catalyst (at 0.10 g) was first pre-treated in a 6 vol% H₂/N₂ (at 30 mL min⁻¹) at 300 °C for 2 h and then cooled down to 120 °C under N₂ flow. Thereafter, pulses of pure oxygen were periodically injected into the reduced catalyst until the saturation was reached.

2.3 Activity measurements

Catalytic activities in toluene oxidation were measured in a fixed-bed tubular reactor (i.d.=8 mm). The catalyst (0.50 g, with grain size in the range of 0.25 to 0.42 mm) was mixed with quartz sand (grain size in the range of 0.25 to 0.42 mm) to yield a total volume of 1 mL. The feed gas (total flow rate at 160 mL min⁻¹) consists of nitrogen carrier gas, reactant gas (500 ppm toluene) and oxygen (10 vol%) and a gas hourly space velocity (GHSV) was maintained at 19200 mL g_{cat}⁻¹ h⁻¹ for all runs without specific indication. The conversion of reactants to various products was evaluated (as a function of temperature) using a gas chromatograph (GC, Agilent Technologies 7890A, USA) equipped with a flame ionization detector (FID). Kinetic measurements were conducted in a kinetic region as proposed in the literature.^{17, 18} The apparent activation energy (E_a) was calculated by applying the Arrhenius plots at fixed temperatures for

each catalyst. The turnover frequencies (TOF) were calculated based on the following equation:

$$TOF_{site} (s^{-1}) = \frac{X_{toluene} \cdot F_{toluene}}{N_{site}}$$

Where $X_{toluene}$ (%) is the toluene conversion at a certain temperature; $F_{toluene}$ ($\mu\text{mol s}^{-1}$) is the flow rate of toluene; N_{site} (μmol) is the number of surface active sites (i.e. noble metal species or superficial oxygen for each catalyst).

3. Results and Discussion

3.1 Phases identification and BET surface area measurements

Phase identities and purities of sc-NiO, sc-Pd/NiO and sc-Pd/NiO-R catalysts were evaluated by using X-ray powder diffraction (XRD). As shown in **Fig. 1**, the sc-NiO catalyst revealed sharp reflections at the 2θ of 37.3, 43.3, 62.9, 75.4 and 79.4°, which were indexed to cubic NiO (pattern JCPDS 73-1523). For sc-Pd/NiO and sc-Pd/NiO-R catalysts, similar reflections to sc-NiO were obtained. However, no reflections assigned to Pd species were observed. The reason could be ascribed to the high dispersion of Pd or the low loading of Pd in the catalysts (the Pd contents were approximately 0.48 wt% and 0.55 wt% for sc-Pd/NiO and sc-Pd/NiO-R, respectively, using ICP-AES). For sc-Pd/NiO, the addition of Pd was found to slightly shift the NiO reflections to lower theta range (as shown in **Fig. 1a**). This suggested that partial Pd^{2+} had been incorporated into the NiO lattice, leading to the expansion of NiO crystal unit (for the Pd^{2+} had a larger ionic radius of 86 pm than the Ni^{2+} of 69 pm). In contrast, the sc-Pd/NiO-R did not show obvious NiO XRD reflection shift, suggesting that the Pd in this catalyst might be isolated with the NiO, which would be further verified by the following XPS and

H₂-TPR analyses. By applying Sherrer's equation, the average crystallite sizes of NiO were calculated at 7.8±0.2 nm, 6.7±0.5 nm and 13.9±1.2 nm for sc-NiO, sc-Pd/NiO and sc-Pd/NiO-R, respectively, which were in line with their surface areas at approximately 150.3, 125.2 and 91.1 m² g⁻¹, respectively.

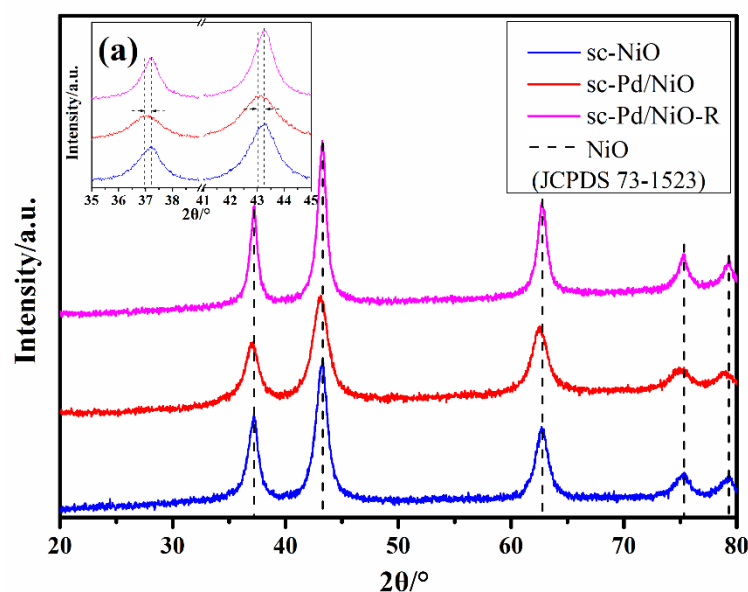


Fig. 1 X-ray diffraction patterns of sc-NiO (JCPDS 73-1523), sc-Pd/NiO and sc-Pd/NiO-R catalysts in the 2 theta range 20 to 80 degrees. (a) represents those with an enlarged coordinate from 35 to 45 degrees to highlight shifts.

The distinct decrease in the surface area for sc-Pd/NiO-R was believed due to its altered reaction condition by the introduction of formic acid, the addition of which was able to lower the super-saturation of Pd and Ni ions¹⁹, thus leading to higher crystallinity (see **Fig. 1**) and larger crystallite size for NiO (and Pd species). The size growth of NiO was also verified by HR-TEM analyses (see supplementary **Fig. S2**), which displayed a hexagonal plate morphology with the particle size at approximately 10.0 nm (based on 100 particle measurements) in sc-NiO and sc-Pd/NiO, whilst for the sc-Pd/NiO-R, a relatively larger size at ca. 15.0 nm was obtained. The Pd species in

either sc-Pd/NiO or sc-Pd/NiO-R were, however, difficult to identify in their HR-TEM. This could be due to the low loadings of Pd in the catalysts. However, the presence of them was verified using STEM-HAADF, showing distinct blue cyan dots of Pd elements highly dispersed over the NiO support (dark field) in either sc-Pd/NiO or sc-Pd/NiO-R catalyst (see supplementary **Fig. S3**).

3.2 Valence state measurements

Fig. 2 illustrated the XPS analyses on the valence states of surficial elements in each catalyst. Generally, the Pd_{3d} XPS spectrum involves the Pd 3d_{5/2} and Pd 3d_{3/2} with a spin-orbit splitting at ca. 5.3 eV. As shown in **Fig. 2a**, the Pd3d_{5/2} spectrum of sc-Pd/NiO displayed three overlapped peaks with the Binding Energy (BE) at approximately 335.7, 337.4 and 339.0 eV, which were ascribed in sequence to metallic Pd⁰, Pd²⁺ and Pd⁴⁺.²⁰ The BE of Pd²⁺ was close to ionic Pd²⁺ (at approximately 337.8 ±0.2 eV)^{8, 21}, suggesting that they were more likely in the ionic form rather than as isolated PdO (BE at approximately 336.5 ±0.2 eV) in the sc-Pd/NiO²². The BE of metallic Pd⁰ displayed approximately 0.5 eV BE shift as compared with the datum value (approximately 335.2 eV)²³. Such a shift was induced by the charge transfer from Pd⁰ to NiO due to the Strong Metal-Support Interaction, SMSI²⁴, which would consequently turn the Pd⁰ into electro-deficient palladium (i.e. “suboxide” PdO_x) as reported by Malyutin et al. and Gabasch et al.^{25, 26}

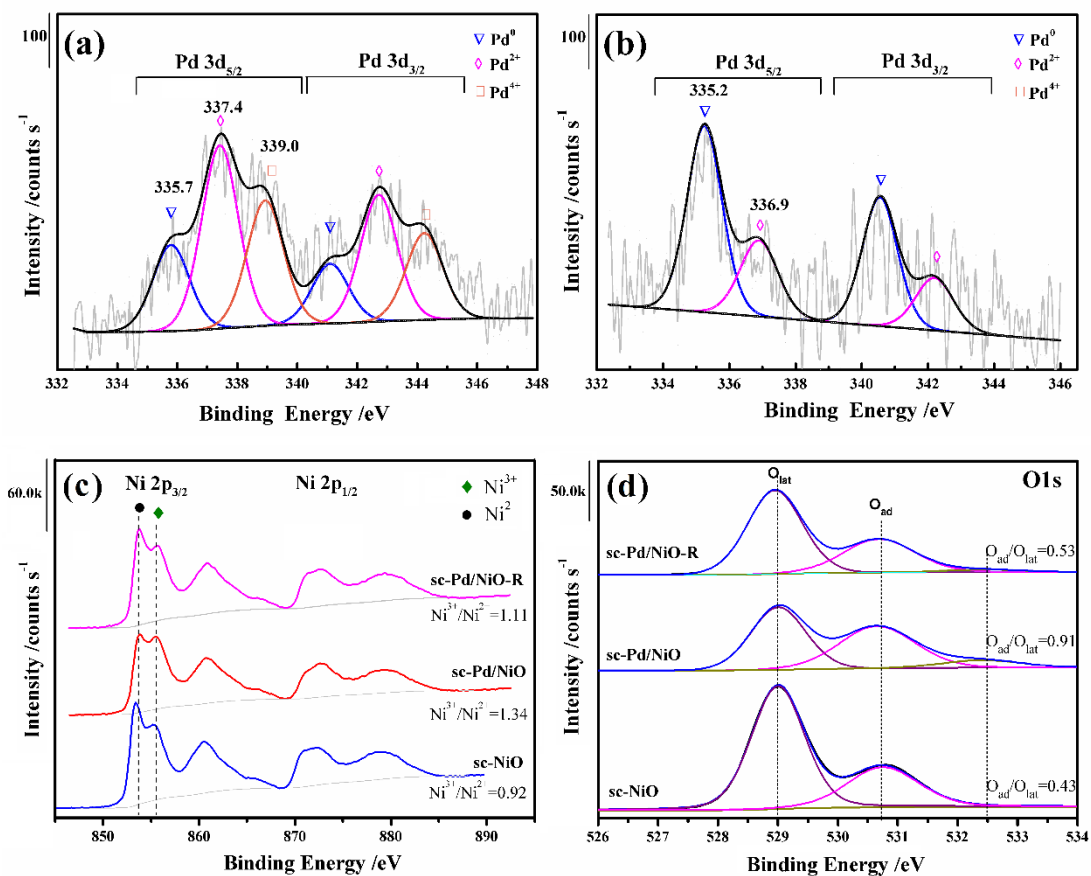


Fig. 2 Pd_{3d} deconvoluted spectra of (a) sc-Pd/NiO and (b) sc-Pd/NiO-R and the Ni2p (c) and O1s (d) spectra of sc-NiO, sc-Pd/NiO and sc-Pd/NiO-R catalysts.

For the sc-Pd/NiO-R, the Pd 3d_{5/2} spectrum (see **Fig. 2b**) only revealed the characteristic BE of Pd⁰ and Pd²⁺. The molar ratio of metallic Pd and all the Pd species (Pd⁰: Pd) was measured at approximately 0.69, which was much higher than that in the sc-Pd/NiO (at approximately 0.22). This result manifested that the sc-H₂O with the ability in dissolving H₂ (and O₂) is indeed capable of adjusting the valence states of noble metals under the hydrothermal synthetic condition. The BE of Pd⁰ in the sc-Pd/NiO-R was measured at 335.2 eV, which was identical to the datum value, suggesting that they were mainly presented as isolated Pd⁰ rather than that as “suboxide” PdO_x in the sc-Pd/NiO.

The Ni2p XPS generally consists of a doublet corresponding to Ni2p_{3/2} and Ni2p_{1/2}, with a spin-orbit splitting of approximately 17.4 eV.²⁷ The Ni2p_{3/2} peak at 853.7 eV (and a satellite signal at ca. 861.0 eV) is correlated with Ni²⁺ and that at 855.6 eV is assigned to Ni³⁺.²⁸ As shown in **Fig. 2c**, the ratios of Ni³⁺:Ni²⁺ were measured in the sequence of sc-Pd/NiO > sc-Pd/NiO-R > sc-NiO. Since the Ni³⁺ was reported to be created by the formation of cation defects in NiO²⁹, the sc-Pd/NiO with the most Ni³⁺ was expected to have the highest amounts of defects amongst investigated catalysts. These defects were believed to be induced by the partial incorporation of Pdⁿ⁺ into the NiO lattice (see XRD reflection shift in **Fig. 1**). **Fig. 2d** displayed three O1s BE peaks at approximately 529.3, 531.0 and 532.5 eV, associating with the surface lattice oxygen, chemisorbed oxygen and hydroxyl (and/or carbonate) species, respectively.³⁰ The ratio of chemisorbed oxygen to lattice oxygen (O_{ad}/O_{lat}) also showed a trend of sc-Pd/NiO > sc-Pd/NiO-R > sc-NiO, which was in line with that of Ni³⁺:Ni²⁺.

3.3 Redox potential measurements

Fig. 3a showed the redox potentials of sc-NiO, sc-Pd/NiO, and sc-Pd/NiO-R catalysts as evaluated by using H₂-TPR. The sc-NiO displayed a broad asymmetrical reduction peak centred at approximately 375 °C, which was believed to be originated from the reduction of Ni³⁺ to Ni²⁺ and further to elemental nickel.^{28, 29} While for sc-Pd/NiO, a much lower NiO reduction peak at approximately 315 °C were observed. Such a promotion in NiO redox potential should be the result of SMSI between Pd and NiO that facilitated the diffusion of dissociated hydrogen to NiO.^{31, 32} The additional peak at approximately 130 °C in the sc-Pd/NiO catalyst should be due to the reduction

of oxidized Pd species^{33, 34}. For the sc-Pd/NiO-R, the NiO reduction peak was centred at approximately 346 °C, which was higher than that in the sc-Pd/NiO. This is rational given that the sc-Pd/NiO-R had the majority of isolate Pd⁰, where the SMSI between Pd and NiO would be much weakened, thus limiting the promotion of redox potential for NiO. However, such a weakened effect was beneficial for the Pd species as the anchoring of which (by NiO) could be to some extent inhibited³⁵. As such, the Pd species in the sc-Pd/NiO-R retained a high redox potential, which yielded a lower H₂ consumption peak at approximately 110 °C than that in the sc-Pd/NiO (at 130 °C). The low-temperature reducibility of NiO was also evaluated by calculating its initial (i.e. 25%) H₂ consumption rate in H₂-TPR. As shown in **Fig. 3b**, the sc-Pd/NiO catalyst still showed the best low-temperature reducibility for NiO.

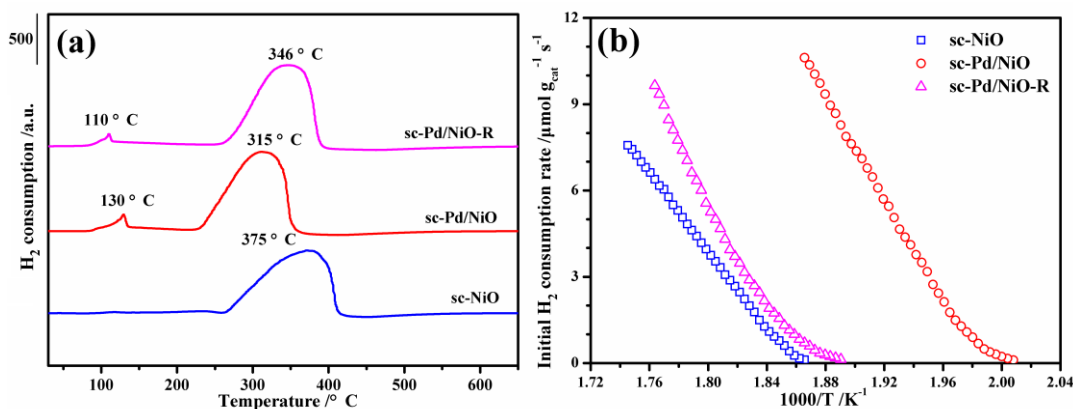


Fig. 3 (a) H₂-TPR profiles and (b) initial H₂ consumption rates of NiO in sc-NiO, sc-Pd/NiO and sc-Pd/NiO-R catalysts. *Conditions: 200 °C O₂/He pre-treatment for 1h, 6 vol% H₂ in N₂ with a flow rate of 50 mL min⁻¹, 0.05 g catalyst and a ramping rate at 5 °C min⁻¹.

3.4 Catalytic activity measurements

The catalytic activities of sc-NiO, sc-Pd/NiO, and sc-Pd/NiO-R in toluene oxidation were evaluated by both measuring the overall toluene conversion rates and calculating the kinetic parameters. For the former, catalysts were subjected to a feed stream containing approximately 500 ppm toluene and excessive O₂ (i.e. 10 vol% O₂) at a GHSV of 19200 mL g_{cat}⁻¹ h⁻¹. Carbon dioxide and water were the main products for toluene oxidation over all the catalysts, and carbon dioxide contributed to approximately 99% as estimated in carbon balance. The result was in line with the reported CO₂ selectivity for NiO based catalyst and noble metal catalysts in the literature.^{24, 28, 36} The CO₂ evolution rates were then used in the light-off curves instead of toluene conversion herein. As shown in **Fig. 4a**, the sc-Pd/NiO yielded a T₉₀ (i.e. temperature at which 90% CO₂ conversion was reached) at approximately 255 °C and a light-off temperature, T₅₀, at approximately 240 °C, which were both lower than those of the sc-NiO. The presence of Pd-NiO interface and high amounts of O_{ad} (see XPS result in **Fig. 2**) in the sc-Pd/NiO should be accounted for such a better performance. The sc-Pd/NiO-R had shown the highest activity amongst investigated catalysts, which yielded the T₉₀ at approximately 190 °C and the T₅₀ at approximately 170 °C. In contrast, the post-treated sample sc-Pd/NiO-H₂ displayed CO₂ evolution rates at higher T₉₀ (210 °C) and T₅₀ (194 °C), inferior to the one-pot synthesized sc-Pd/NiO-R as shown in Supplementary **Fig. S4**. The sintering/encapsulation of surface-active particles during the post-treatment could account for such an inferior activity for toluene oxidation.

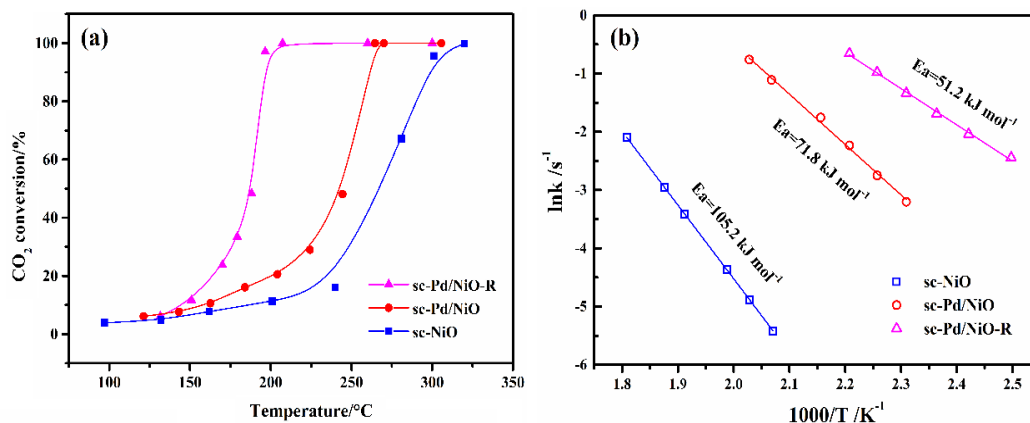


Fig. 4 (a) Carbon dioxide conversion rates versus temperature and (b) Arrhenius plots for sc-NiO, sc-Pd/NiO and sc-Pd/NiO-R catalysts.

*(a) Conditions: toluene (500 ppm), O₂ (10 vol%), GHSV = 19200 mL g_{cat}⁻¹ h⁻¹.

(b) Conditions: toluene (500 ppm), O₂ (10 vol%), GHSV = 60000 mL g_{cat}⁻¹ h⁻¹.

In the kinetic measurement, a GHSV value of 60000 mL g_{cat}⁻¹ h⁻¹ was selected based on the Weisz-Prater criteria to eliminate the mass transfer limit at lower conversions (less than 5-15%).^{37, 38} It has been assumed that toluene oxidation in the presence of excessive oxygen (toluene/O₂ molar ratio = 1/200) over our investigated catalysts would follow a first-order reaction mechanism^{23, 38} with respect to toluene concentration (c): $r = -k c = (-A \exp(-E_a/RT)) c$, where r is the reaction rate (mol s⁻¹), k the rate constant (s⁻¹), A the pre-exponential factor, and E_a the apparent activation energy (kJ mol⁻¹). The values of k were calculated according to initial reaction rates at fixed temperatures. As shown in **Fig. 4(b)**, the Arrhenius plots for sc-NiO, sc-Pd/NiO and sc-Pd/NiO-R all displayed a linear dependence, indicating that the assumption of first-order reaction mechanism was appropriate. The E_a value for sc-NiO was calculated at approximately 105.2 kJ mol⁻¹, which was similar to many reported metal oxide catalysts, e.g. CuO/Al₂O₃ or MnO/Al₂O₃ (the E_a were reported in the range of

approximately 96 to 120 kJ mol⁻¹)³⁹. As compared, the sc-Pd/NiO displayed a much lower E_a (at approximately 71.8 kJ mol⁻¹), an even lower value than that of the Au/Co₃O₄ (in the range 74 to 84 kJ mol⁻¹)⁴⁰ and Pd/C (approximately 83 kJ mol⁻¹)¹⁰ in the literature. While for the sc-Pd/NiO-R, the lowest E_a at approximately 51.2 kJ mol⁻¹ was obtained, in line with their activity measurements.

From the activity and kinetic measurements, it seems that the Pd⁰ is more active than the PdO_x in toluene oxidation. In general, the oxidation of toluene can follow either Langmuir-Hinshelwood (L-H) or Mars-van Krevelen (M-K) mechanism^{4, 10, 38}, where toluene adsorbs at the catalytic site and reacts with either dissociated gaseous oxygen or surface lattice oxygen to form CO₂ and H₂O. In our Pd/NiO-R catalyst, the catalytic sites for toluene adsorption/activation were originally considered to be Pd⁰ (where the PdO_x should be not able to adsorb toluene); this process involved either the electron transfer from aromatic ring to Pd⁰ or the deprotonation of methyl group at the Pd⁰.^{41, 42} However, after introducing toluene to the sc-NiO at room temperature, the DRIFT spectra (see supplementary **Fig. S5**) showed the appearance of bands centered at 1734, 1548, 1459, 1365 cm⁻¹, which were indexed to benzaldehyde/benzoic acid^{43, 44}. Obviously, the NiO could also adsorb/activate toluene at low temperatures; this process was through the attack on the carbon atom of methyl by the active oxygen in NiO⁴⁵. As such, the adsorption/activation of toluene might not be the main factor accounting for such a distinct activity difference between sc-Pd/NiO-R and sc-Pd/NiO, and the adsorption/activation of gaseous oxygen could be the critical factor in determining their performances.⁴⁶⁻⁴⁸

To verify this, temperature-programmed surface reaction (TPSR) measurement was then conducted; the catalyst was subjected to a flow of 5 vol% O₂/He at elevated temperatures and the desorbed O₂ in the outlet gas was simultaneously measured using an MS. As shown in **Fig. 5**, the sc-Pd/NiO did not show any oxygen uptake in the temperature range of 20-200 °C, which indicated that the Pd species in this catalyst (mainly present as “suboxide” PdO_x and oxide PdO, see XPS analyses in **Fig. 2**) were unable to dissociate the gaseous oxygen at low temperatures. As such, the dissociation of them should be mainly through the NiO at relatively high temperatures, where the PdO_x might be functioned to assist the spillover of the dissociated oxygen from NiO to enhance toluene oxidation⁴⁹. While for the sc-Pd/NiO-R, a distinct oxygen uptake was observed. The consumption of oxygen started at approximately 115 °C, following by a peak emerging at approximately 160 °C. Apparently, the sc-Pd/NiO-R that was with the majority of isolate Pd⁰ was able to dissociate the gaseous oxygen at low temperatures^{47, 50}; this might explain why the catalyst had a much higher activity than the sc-Pd/NiO for toluene oxidation.

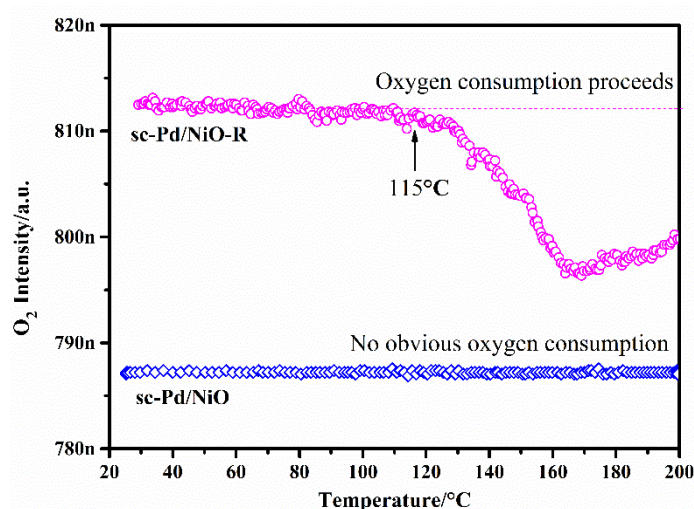


Fig. 5 Temperature-programmed oxygen reaction over fresh catalysts in a range of 20 to 200°C. The plot shows the oxygen consumption for sc-Pd/NiO-R from approximately 115°C onwards. *Condition: 5% O₂ in He with a flow rate of 50 mL min⁻¹, 0.1g catalyst and a ramping rate at 2 °C min⁻¹.

One might argue that the highly dispersed Pd⁰ (see Supplementary **Fig. S3** for STEM-XEDS mapping) in the sc-Pd/NiO-R might incline to be oxidized and not be able to restore into Pd⁰ in the excess of oxygen. To verify this, we then introduced approximately 500 ppm toluene stream into the O₂-pretreated sc-Pd/NiO-R catalyst. As shown in **Fig. 6**, a distinct desorption of CO₂ appeared at the same temperature of oxygen uptake (approximately 110°C). This implied that an instant reaction occurred once the toluene in contact with the Pd. Such a reaction would restore the oxidized Pd into Pd⁰ and retained the redox cycle for toluene oxidation. To verify the oxidation state of Pd under operating conditions, we also characterized the XPS on a used sc-Pd/NiO-R catalyst (being aged during the catalytic performance). As shown in Supplementary **Fig. S6**), the aged catalyst still showed the characteristic BE of Pd⁰ at 335.3 eV, similar to the fresh sc-Pd/NiO-R catalyst and the molar ratio of Pd⁰: Pd reached equilibrium at 0.5 (slightly lower than 0.69 in the fresh counterpart). Such a result manifested the ability of sc-Pd/NiO-R in restoring into metallic valence with excessive oxygen although partial of Pd⁰ could be oxidized.

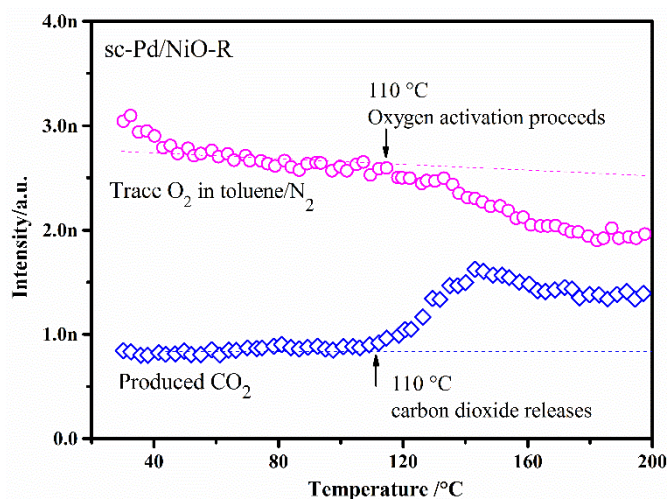


Fig. 6 Temperature-programmed reaction data in a range of 20 to 200 °C for toluene oxidation (without oxygen gas feeding) over oxidized sc-Pd/NiO-R. The plot shows the carbon dioxide was produced from approximately 110°C onwards. *Condition: 500 ppm toluene in N₂ with a flow rate of 50 mL min⁻¹, 0.1g catalyst and a ramping rate at 2 °C min⁻¹.

While for the sc-Pd/NiO (see **Fig. 7**), the catalyst was found to desorb oxygen at the temperature of approximately 70 °C. These oxygen species then oxidized the toluene, leading to a CO₂ desorption hump centred at approximately 165 °C. It seemed that under such a reducing atmosphere (i.e. only toluene introduced), the sc-Pd/NiO was capable of oxidizing the toluene at low temperatures. Considering the different reaction conditions between the TPSR in **Fig. 6** (and **Fig. 7**) and that in **Fig. 5** (with excessive O₂), we deduced that the PdO and PdO_x might be difficult to convert into metallic Pd⁰ in the excess of oxygen. As such, the gaseous oxygen dissociation process over the sc-Pd/NiO would be blocked, which thus led to a less active performance in toluene oxidation (see **Fig. 4**). As confirmed, no existence of exposed metallic Pd⁰ (with

the BE at 335.2 eV) was observed for both the fresh and used sc-Pd/NiO (data were not shown here).

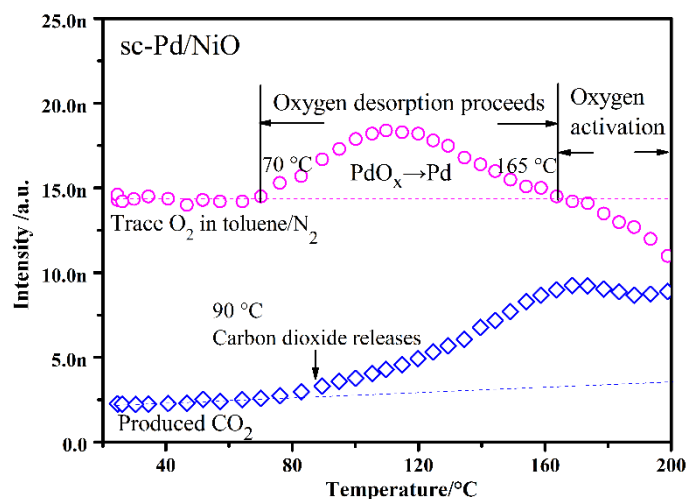


Fig. 7 Temperature-programmed reaction data in a range of 20 to 200 °C for toluene oxidation (without oxygen gas feeding) over oxidized sc-Pd/NiO. The plot shows oxygen desorption from approximately 70 °C and carbon dioxide release from approximately 90 °C onwards. *Condition: 500 ppm toluene in N₂ with a flow rate of 50 mL min⁻¹, 0.1g catalyst and a ramping rate at 2 °C min⁻¹.

Based on the explored mechanisms, the turnover frequencies (TOF_(O) and TOF_(Pd), respectively) for sc-Pd/NiO and sc-Pd/NiO-R catalysts in toluene oxidation were calculated. The active site of sc-Pd/NiO-R was designed as Pd⁰, which was calculated based on the amounts of Pd (as measured by ICP-AES, i.e. 0.55 wt%) multiplied by 0.5 (i.e. the Pd⁰:Pd ratio in the aged catalyst as measured by XPS, see Supplementary **Fig. S6**). Note: since the NiO could also adsorb H₂ or CO at low temperatures, we were not able to measure the surface dispersion rate of Pd in the sc-Pd/NiO-R by using either H₂ or CO chemisorption method. Therefore, all Pd species were involved in TOF calculation. The active species of sc-Pd/NiO were considered to be surface chemisorbed

oxygen at NiO (and/or Pd-NiO interface), the number of which, $N_{(O)}$, was calculated by using the equation:

$$N_{(O)} = \text{OSC}_{\text{surface}} - \text{OSC}_{\text{Pd}}$$

Where the $\text{OSC}_{\text{surface}}$ represents the total amounts of chemisorbed oxygen at the sc-Pd/NiO catalyst surface, which was measured by using a pulse hydro-oxygen titration (HOT) method (see Supplementary **Fig. S7**) and the OSC_{Pd} represents for the oxygen dissociation by all Pd species (considering one Pd-H atom adsorbing 3/2 O atoms, i.e. $2\text{PdH} + 3/2\text{O}_2 = \text{H}_2\text{O} + 2\text{PdO}$). At a selected temperature of 160 °C, the $\text{TOF}_{(O)}$ for sc-Pd/NiO was calculated at approximately $0.8 \times 10^{-4} \text{ s}^{-1}$, which was one order of magnitude lower than the $\text{TOF}_{(\text{Pd})}$ of sc-Pd/NiO-R at $1.0 \times 10^{-3} \text{ s}^{-1}$.

In sum, we unveil that the Pd^0 is more active than PdO_x and transition metal oxides in the catalytic oxidation of toluene. This is because the Pd^0 is capable of dissociating gaseous oxygen at low temperatures and recovering to original chemical state even in the excess of oxygen. The PdO_x , although could desorb active oxygen under a reducing atmosphere and might assist the oxygen spillover from NiO, is difficult to convert into Pd^0 in an oxygen-rich environment. It seems that for noble metal catalysts, the metallic state and the ability in restoring to this state play a crucial role in VOCs oxidation; the former could effectively activate both toluene and gaseous oxygen at low temperatures and the latter could retain the redox cycle for VOCs oxidation. This explains why somehow the larger particle of noble metal had a much better activity than the small one in VOCs oxidation as the former is rather difficult to be oxidized and thus easy to retain its metallic state.^{33, 51}

3.5 Durable activity and low noble metal loading

Durability always remains a major concern for industrial catalysts toward VOCs oxidation. To elucidate the durability of sc-Pd/NiO-R catalyst, the catalyst was then subjected to an increasing GHSV from 19200 to 180000 mL g_{cat}⁻¹ h⁻¹. As shown in **Fig. 8a**, the T₅₀ of this catalyst was retained less than 220 °C when the GHSV was drastically increased to 180000 mL g_{cat}⁻¹ h⁻¹. After ageing the sc-Pd/NiO-R catalyst at approximately T₆₀ (190 °C) and T₉₅ (200 °C) for 25 h, respectively, both the conversions of toluene and CO₂ did not show any obvious decline (see supplementary **Fig. S8**). We also introduced 5 vol% H₂O in the reaction system to simulate a real exhaust condition for sc-Pd/NiO-R. The water-resistant ability and durable activity after repeated cycles and isothermal ageing at approximately 194 °C for 25 h were conducted, the results of which were illustrated in **Fig. S9**. No deactivation was observed during both the ageing test, manifesting the sc-Pd/NiO-R catalyst with a stable catalytic performance even with 5 vol.% water vapour.

Furthermore, lowering the loading amount of Pd (see **Fig. 8b**) did not cause distinct activity decline for sc-Pd/NiO-R catalyst. The loading of 0.43 wt% Pd even displayed a relatively higher activity than the 0.55 wt% one. The reason could be due to the less loading that resulted in the higher dispersion of Pd over the NiO as further increasing the loading to 0.64 wt% had led to an even worse catalytic performance. This result further reveals the importance of optimizing loading of noble metals in VOCs oxidation for practical applications.

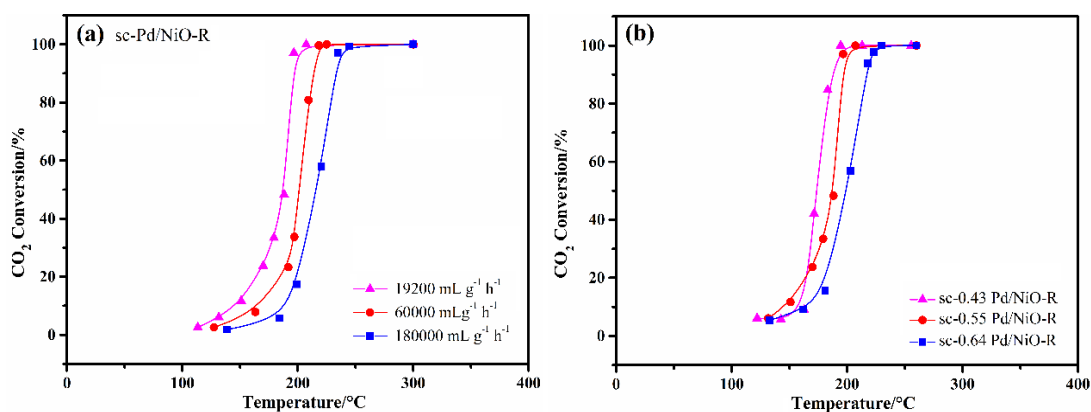


Fig. 8 Carbon dioxide conversion rates of sc-Pd/NiO-R for toluene oxidation (a) with a constant loading amount (0.55 wt%) at varied GHSV and (b) with different Pd loading amount at a GHSV of $19200 \text{ mL g}_{\text{cat}}^{-1} \text{ h}^{-1}$. *Condition: toluene (500 ppm), O_2 (10 vol.%), 0.5 g catalyst.

4 Conclusions

In this article, we used sc- H_2O as a feasible reaction medium for facile syntheses and *in situ* valence modification of Pd/NiO hybrid nano-catalysts for toluene oxidation. The high solubility of O_2/H_2 in the sc- H_2O assured a two-phase reaction between Pd and dissolved O_2/H_2 , which led to an *in situ* modification of Pd valence under the hydrothermal condition. We unveil that the Pd^0 is more active than PdO_x and transition metal oxides in the catalytic oxidation of toluene, owing to its capability of dissociating gaseous oxygen (and/or activating toluene) at low temperatures even in the excess of oxygen. This work, particularly the developed route for *in situ* valence modification and the explored mechanistic function for noble metal valence, could provide practical guidance for the development of low-temperature activated hybrid nano-catalysts with low precious metal loadings for industry.

Conflicts of interest

There are no conflicts to declare.

Acknowledgements

This work was financially supported by the National Natural Science Foundation of China (Grant No. 51478418) and the Program for Zhejiang Leading Team of S&T Innovation (Grant No. 2013TD07).

References

1. J. Fenger, *Atmos. Environ.*, 2009, **43**, 13-22.
2. J. W. S. Longhurst, J. G. Irwin, T. J. Chatterton, E. T. Hayes, N. S. Leksmono and J. K. Symons, *Atmos. Environ.*, 2009, **43**, 64-78.
3. B. de Rivas, R. Lopez-Fonseca, C. Jimenez-Gonzalez and J. I. Gutierrez-Ortiz, *J. Catal.*, 2011, **281**, 88-97.
4. Z. Zhang, Z. Jiang and W. Shangguan, *Catal. Today*, 2016, **264**, 270-278.
5. J. I. Gutierrez-Ortiz, B. de Rivas, R. Lopez-Fonseca and J. R. Gonzalez-Velasco, *Appl. Catal., B*, 2006, **65**, 191-200.
6. R. Peng, X. Sun, S. Li, L. Chen, M. Fu, J. Wu and D. Ye, *Chem. Eng. J.*, 2016, **306**, 1234-1246.
7. W. Z. Si, Y. Wang, S. Zhao, F. Y. Hu and J. H. Li, *Environ. Sci. Technol.*, 2016, **50**, 4572-4578.
8. P. Li, C. He, J. Cheng, C. Y. Ma, B. J. Dou and Z. P. Hao, *Appl. Catal., B*, 2011, **101**, 570-579.

9. H. L. Tidahy, S. Siffert, J. F. Lamonier, E. A. Zhilinskaya, A. Aboukais, Z. Y. Yuan, A. Vantomme, B. L. Su, X. Canet, G. De Weireld, M. Frere, T. B. N'Guyen, J. M. Giraudon and G. Leclercq, *Appl. Catal., A*, 2006, **310**, 61-69.
10. J. Bedia, J. M. Rosas, J. Rodriguez-Mirasol and T. Cordero, *Appl. Catal., B*, 2010, **94**, 8-18.
11. K. Okumura, T. Kobayashi, H. Tanaka and M. Niwa, *Appl. Catal., B*, 2003, **44**, 325-331.
12. J. A. Darr and M. Poliakoff, *Chem. Rev.*, 1999, **99**, 495-541.
13. X. L. Weng, J. Y. Zhang, Z. B. Wu and Y. Liu, *Catal. Today*, 2011, **175**, 386-392.
14. E. Lester, P. Blood, J. Denyer, D. Giddings, B. Azzopardi and M. Poliakoff, *J. Supercrit. Fluids*, 2006, **37**, 209-214.
15. T. Honma and H. Inomata, *Fluid Phase Equilib.*, 2007, **257**, 238-243.
16. Y. C. Zhang, J. Zhang, L. Zhao and C. D. Sheng, *Energy Fuels*, 2010, **24**, 95-99.
17. W. Wang, Q. Meng, X. Weng and Z. Wu, *Catal. Commun.*, 2016, **84**, 167-170.
18. Q. Meng, W. Wang, X. Weng, Y. Liu, H. Wang and Z. Wu, *J. Phys. Chem. C*, 2016, **120**, 3259-3266.
19. S. Kubota, T. Morioka, M. Takesue, H. Hayashi, M. Watanabe and R. L. Smith, Jr., *J. Supercrit. Fluids*, 2014, **86**, 33-40.
20. M. Moroseac, T. Skála, K. Veltruská, V. Matolín and I. Matolínová, *Surf. Sci.*, 2004, **566–568, Part 2**, 1118-1123.

21. C. Du, Y. Guo, Y. Guo, X.-q. Gong and G. Lu, *J. Mater. Chem. A*, 2015, **3**, 23230-23239.
22. T. Baidya, K. R. Priolkar, P. R. Sarode, M. S. Hegde, K. Asakura, G. Tateno and Y. Koike, *J. Chem. Phys.*, 2008, **128**.
23. Z. Wu, J. Deng, S. Xie, H. Yang, X. Zhao, K. Zhang, H. Lin, H. Dai and G. Guo, *Microporous Mesoporous Mater.*, 2016, **224**, 311-322.
24. X. L. Weng, D. D. Tan, X. L. Cao, J. Y. Zhang and Z. B. Wu, *Catal. Sci. Technol.*, 2016, **6**, 2901-2904.
25. A. V. Malyutin, A. I. Mikhailichenko, Y. V. Zubavichus, V. Y. Murzin, A. G. Koshkin and I. V. Sokolov, *Kinet. Catal.*, 2015, **56**, 89-105.
26. H. Gabasch, A. Knop-Gericke, R. Schloegl, M. Borasio, C. Weilach, G. Rupprechter, S. Penner, B. Jenewein, K. Hayek and B. Kloetzer, *Phys. Chem. Chem. Phys.*, 2007, **9**, 533-540.
27. Y. Song, X. Zhang, S. Yang, X. Wei and Z. Sun, *Fuel*, 2016, **181**, 269-276.
28. G. Bai, H. Dai, J. Deng, Y. Liu and K. Ji, *Catal. Commun.*, 2012, **27**, 148-153.
29. F. Yu, X. Xu, H. Peng, H. Yu, Y. Dai, W. Liu, J. Ying, Q. Sun and X. Wang, *Appl. Catal., A*, 2015, **507**, 109-118.
30. B. Agula, Q.-F. Deng, M.-L. Jia, Y. Liu, B. Zhaorigetu and Z.-Y. Yuan, *React. Kinet., Mech. Catal.*, 2011, **103**, 101-112.
31. S. Colussi, A. Gayen, M. F. Camellone, M. Boaro, J. Llorca, S. Fabris and A. Trovarelli, *Angew. Chem., Int. Ed.*, 2009, **48**, 8481-8484.

32. Y. Z. Li, Y. N. Fan, H. P. Yang, B. L. Xu, L. Y. Feng, M. F. Yang and Y. Chen, *Chem. Phys. Lett.*, 2003, **372**, 160-165.
33. A. Baylet, P. Marecot, D. Duprez, P. Castellazzi, G. Groppi and P. Forzatti, *Phys. Chem. Chem. Phys.*, 2011, **13**, 4607-4613.
34. M. Hosseini, T. Barakat, R. Cousin, A. Aboukais, B. L. Su, G. De Weireld and S. Siffert, *Appl. Catal., B*, 2012, **111**, 218-224.
35. H. L. Tidahy, M. Hosseni, S. Siffert, R. Cousin, J. F. Lamonier, A. Aboukais, B. L. Su, J. M. Giraudon and G. Leclercq, *Catal. Today*, 2008, **137**, 335-339.
36. X. Weng, J. Zhang, Z. Wu, Y. Liu, H. Wang and J. A. Darr, *Green Chem.*, 2011, **13**, 850-853.
37. H. Arandiyani, H. Dai, J. Deng, Y. Wang, H. Sun, S. Xie, B. Bai, Y. Liu, K. Ji and J. Li, *J. Phys. Chem. C*, 2014, **118**, 14913-14928.
38. S. Xie, J. Deng, S. Zang, H. Yang, G. Guo, H. Arandiyani and H. Dai, *J. Catal.*, 2015, **322**, 38-48.
39. S. M. Saqer, D. I. Kondarides and X. E. Verykios, *Appl. Catal., B*, 2011, **103**, 275-286.
40. S. Xie, H. Dai, J. Deng, Y. Liu, H. Yang, Y. Jiang, W. Tan, A. Ao and G. Guo, *Nanoscale*, 2013, **5**, 11207-11219.
41. L. F. Liotta, *Appl. Catal., B*, 2010, **100**, 403-412.
42. M. Chen, Y. Ma, G. Li and X. Zheng, *Catal. Commun.*, 2008, **9**, 990-994.
43. G. Busca, F. Cavani and F. Trifirò, *J. Catal.*, 1987, **106**, 471-482.
44. M. Sanati and A. Andersson, *J. Mol. Catal.*, 1993, **81**, 51-62.

45. L. Liu, Y. Song, Z. Fu, Q. Ye, S. Cheng, T. Kang and H. Dai, *Appl. Surf. Sci.*, 2017, **396**, 599-608.
46. H. Huang and D. Y. C. Leung, *ACS Catal.*, 2011, **1**, 348-354.
47. C. He, J. Li, X. Zhang, L. Yin, J. Chen and S. Gao, *Chem. Eng. J.*, 2012, **180**, 46-56.
48. H. L. Tidahy, S. Siffert, F. Wyrwalski, J. F. Lamonier and A. Aboukaïs, *Catal. Today*, 2007, **119**, 317-320.
49. A. R. Puigdollers, P. Schlexer, S. Tosoni and G. Pacchioni, *ACS Catal.*, 2017, **7**, 6493-6513.
50. H. L. Tidahy, S. Siffert, J. F. Lamonier, R. Cousin, E. A. Zhilinskaya, A. Aboukais, B. L. Su, X. Canet, G. De Weireld, A. Frere, J. M. Giraudon and G. Leclercq, *Appl. Catal., B*, 2007, **70**, 377-383.
51. S. C. Kim and W. G. Shim, *Appl. Catal., B*, 2009, **92**, 429-436.